Chinese Journal of
POLYMER SCIENCE

RESEARCH ARTICLE

https://doi.org/10.1007/s10118-026-3752-0
Chinese J. Polym. Sci.

Thermoplastic Liquid Crystal Elastomers Based on ABA-type Triblock Copolymers

Heng-Hui Zhu, Jin-Yu Wang, Nan-Kai Deng, Jia-Xiang Huang, Ya-Nan Hou, Meng Wang, Zhi-Yang Liu, and Shuai Huang*

School of Chemistry and Chemical Engineering, Southeast University, Nanjing 211189, China

Electronic Supplementary Information

Abstract Liquid crystal elastomers (LCEs) are compelling smart materials for soft robotics and flexible electronics. However, both conventional and dynamically crosslinked LCE systems fundamentally rely on chemically crosslinked networks, which has long been regarded as a prerequisite for their reversible actuation. While thermoplastic elastomers based on block copolymers offer a structural model for constructing robust physically crosslinked networks, it remains a significant challenge to transplant this design strategy into LCEs to realize reversible actuation in non-covalently crosslinked system. Herein, we develop a physically crosslinked thermoplastic LCE system based on ABA-type triblock copolymers (PS-*b*-MCLCP-*b*-PS). Polystyrene (PS) hard-block aggregates act as reversible physical crosslinking sites, effectively replacing permanent covalent bonds. We systematically investigated the regulatory effect of the PS block content on the microstructure, mechanical properties, and thermally responsive actuation of the materials. By achieving an optimal balance between physical network confinement and the segment mobility of the liquid crystal phase, the resultant elastomer exhibits excellent reversible thermally driven actuation, well-balanced mechanical properties and solvent recyclability with high mechanical retention. Furthermore, the material demonstrates prominent wide-temperature-range damping performance attributed to the synergistic energy dissipation of the physical network and mesogen rotation. This work offers a feasible molecular design strategy for sustainable and multifunctional LCEs to break the dependence on chemical crosslinking for reversible actuation.

Keywords Liquid crystal elastomer; Block copolymer; Soft actuator; Reversible thermo-responsive deformation

Citation: Zhu, H. H.; Wang, J. Y.; Deng, N. K.; Huang, J. X.; Hou, Y. N.; Wang, M.; Liu, Z. Y.; Huang, S. Thermoplastic liquid crystal elastomers based on ABA-type triblock copolymers. *Chinese J. Polym. Sci.* https://doi.org/10.1007/s10118-026-3752-0

INTRODUCTION

Liquid crystal elastomers (LCEs), as typical stimuli-responsive smart materials, integrate the anisotropic characteristics of mesogens with the high elasticity of the polymer networks.[1,2] Owing to their unique structure, LCEs can undergo significant and reversible macroscopic deformation in response to external stimuli, such as heat and light, thus exhibiting great application potential in cutting-edge fields, including soft robotics,[3–7] artificial muscles,[8,9] and flexible wearable devices.[10,11] To impart LCEs with self-healing and reprocessing capabilities, the construction of dynamic covalent crosslinking networks has emerged as a highly promising strategy.[12–19] Notably, both conventional and dynamic LCE systems are based on chemically crosslinked polymer networks, which were previously regarded as prerequisites for the reversible deformation of LCEs. In contrast, the stimulus-responsive deformation of linear liquid crystal polymers (LCPs) is typically an irreversible one-way process because their uncrosslinked molecular chains would easily slip to generate plastic deformation. Consequently, despite the advantages of facile processing without specific catalysts and a broad processing window, linear LCPs are rarely used in the design of liquid crystal actuators unless a high molecular weight is achieved to form sufficient chain entanglement.[20]

Thermoplastic elastomers based on block copolymers (BCPs) provide an excellent design example, where the hard nanodomains formed by microphase separation act as physical crosslinking points, whereas the soft nanodomains provide the material with elasticity and flexibility.[21–24] This ingenious structure enables the reversible dissociation and reconstruction of physically crosslinked networks merely through heating or solvent treatment, without the need for additional catalysts, thus endowing the materials with excellent reprocessing ability. In addition, nanostructured ABA-type triblock thermoplastic elastomers have been demonstrated to achieve actuation performances that far surpass those of natural skeletal muscles, showing great potential for soft actuators and flexible wearable devices.[25–27] However, it remains a great challenge to transplant the design strategy of BCP-based thermoplastic elastomers into the molecular design of

* Corresponding author, E-mail: huangshuai1991@seu.edu.cn
Invited Research Article
Received April 15, 2026; Accepted May 19, 2026; Published online July 20, 2026

LCEs and realize reversible actuation of non-covalently crosslinked LCEs.

Herein, we demonstrate that linear ABA-type liquid crystalline block copolymers (LCBCPs) can act as thermoplastic LCEs without chemical crosslinking (Fig. 1a). The designed LCBCP is composed of a main-chain LCP (MCLCP) as the middle soft block and polystyrene (PS) as the two hard end blocks. The PS hard domains serve as reversible physical crosslinking sites (Fig. 1b), whereas the MCLCP middle block forms a stimulus-responsive elastic domain. To realize reversible thermally driven deformation, we optimized the polymeric structure to achieve a delicate balance between physical confinement from the PS crosslinking domains and the segment mobility of the MCLCP phase. We also systematically investigated the structure-property relationship of the materials and demonstrated their potential applications in soft actuators and damping materials. This work provides an unconventional design example for thermoplastic LCEs that does not rely on chemically crosslinked networks for the development of sustainable LCE materials.

EXPERIMENTAL

Materials

2,2′-(Ethylenedioxy)diethanethiol (DODT) and 2-hydroxyethyl methacrylate (HEMA) were purchased from Aladdin (Shanghai) Inc. 1,4-Bis-[4-(3-acryloyloxypropyloxy)benzoyloxy]-2-methylbenzene (RM257) and tris(2-pyridylmethyl)amine (TPMA) were purchased from Bide (Shanghai) Co., Ltd. Triethylamine (TEA) was purchased from Saan (Shanghai) Chemical Technology Co., Ltd. 2-Bromoisobutyryl bromide (BIBB) was purchased from Meryer (Shanghai) Biochemical Co., Ltd. Styrene and tin(II) 2-ethylhexanoate (stannous octoate) were purchased from Adamas Reagent Co., Ltd. (Shanghai, China). Copper(II) bromide ($CuBr_2$) was purchased from J&K Scientific (Beijing) Co., China). All the reagents and solvents were used as received without further purification.

Synthesis of MCLCP Initiators

The molecular weights of the MCLCP initiators were adjusted by changing the molar ratio of the LC monomer to the chain extender. The synthesis of Br-MCLCP$_{31}$-Br was described as a representative example. A thiol-terminated MCLCP was first synthesized *via* thiol-ene click reaction: LC monomer RM257 (5.8860 g, 10.00 mmol) was dissolved in 10 mL of dichloromethane (DCM), and then 3,6-dioxa-1,8-octanedithiol (DODT, total 1.8963 g, 10.40 mmol) was added in three batches (1.7063 g, 9.36 mmol; 0.0950 g, 0.52 mmol; 0.0950 g, 0.52 mmol) at 12 h intervals, with triethylamine (TEA, 30 μL) as the catalyst. The resulting solution was diluted with DCM (10 mL), followed by the addition of HEMA (0.1952 g, 1.50 mmol) and TEA (20 μL). The mixture was stirred at room temperature for 12 h to afford a hydroxyl-terminated MCLCP intermediate, which was purified *via* reprecipitation in methanol and dried under vacuum. Finally, the target bromine-terminated MCLCP macroinitiator was prepared *via* esterification between the hydroxyl-terminated MCLCP intermediate and 2-bromoisobutyryl bromide (BIBB, 0.1380 g, 0.60 mmol). The product was further purified *via* precipitation in excess methanol and dried under vacuum at 35 °C for 24 h to obtain Br-MCLCP$_{31}$-Br.

Synthesis of the Triblock Copolymer (PS-*b*-MCLCP-*b*-PS)

A series of PS-*b*-MCLCP-*b*-PS were synthesized *via* atom transfer

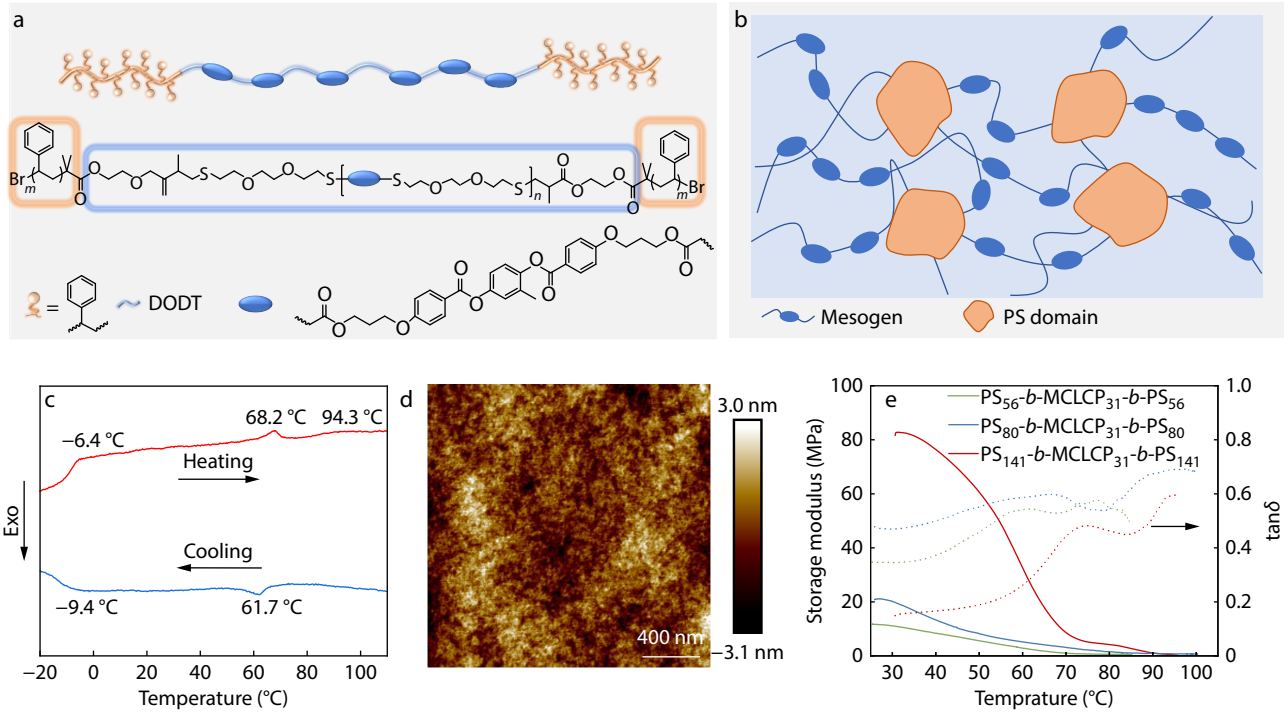

Fig. 1 (a) Chemical structure of PS-*b*-MCLCP-*b*-PS; (b) Schematic illustration of the physically-crosslinked structure; (c) DSC curves of PS_{80}-*b*-$MCLCP_{31}$-*b*-PS_{80} recorded at the second heating-cooling cycle; (d) AFM height image of PS_{80}-*b*-$MCLCP_{31}$-*b*-PS_{80}; (e) DMA profiles of PS_{56}-*b*-$MCLCP_{31}$-*b*-PS_{56}, PS_{80}-*b*-$MCLCP_{31}$-*b*-PS_{80}, and PS_{141}-*b*-$MCLCP_{31}$-*b*-PS_{141}.

https://doi.org/10.1007/s10118-026-3752-0

radical polymerization (ATRP) by adjusting the molar ratio of the macromolecular initiator Br-MCLCP-Br to the styrene monomer. The synthesis of PS_{80}-*b*-$MCLCP_{31}$-*b*-PS_{80} was described as a representative example. $CuBr_2$ (0.0112 g, 0.05 mmol) and TPMA (0.1456 g, 0.50 mmol) with a molar ratio of 1:10 were dissolved in 2 mL of 1,2-dichloroethane (DCE) to prepare a dark green catalyst solution (5.6 mg/mL). The as-synthesized Br-$MCLCP_{31}$-Br macroinitiator (4.7602 g, 0.20 mmol, M_n=23.8 kDa) was dissolved in DCE under magnetic stirring, followed by the addition of styrene (3.1735 g, 30.40 mmol, 40 wt% relative to the macroinitiator). Then 64 μL of the above $CuBr_2$/TPMA catalyst solution (containing 3.6 mg, 0.016 mmol of $CuBr_2$) was added to the macroinitiator/styrene solution. The mixture was purged with dry nitrogen for 20 min to remove oxygen, and then a DCE solution of $Sn(Oct)_2$ (0.0972 g, 0.24 mmol) was injected. Three freeze-pump-thaw cycles were performed to ensure a strictly oxygen-free environment, and ATRP was initiated in an oil bath at 80 °C for 18 h. After polymerization, the crude product was diluted with DCM, filtered through a short column packed with neutral alumina and silica gel to remove the catalyst, precipitated in excess methanol, and dried under vacuum at 35 °C for 24 h to obtain the pale-yellow PS_{80}-*b*-$MCLCP_{31}$-*b*-PS_{80} triblock copolymer.

Characterizations

All ^{1}H-NMR spectra were recorded using a Bruker HW600 MHz spectrometer (AVANCE AV-600). The number-average molecular weight (M_n) and polydispersity index (PDI) of the polymers were determined by gel permeation chromatography (GPC, Agilent PL-GPC 220) using tetrahydrofuran (THF) as the eluent. Differential scanning calorimetry (DSC) measurements were conducted on a TA Q20 instrument (New Castle, DE, USA) under a nitrogen atmosphere, with a temperature range from −40 °C to 130 °C and a heating/cooling rate of 10 °C/min. The second heating curve was used for data analysis to eliminate the thermal history of the samples. Thermogravimetric analysis (TGA) was performed on a Perkin-Elmer TGA7 instrument under nitrogen at a heating rate of 10 °C/min over a temperature range of 30–600 °C. The microphase-separation morphology of the materials was observed *via* atomic force microscopy (AFM, ICON) after spin-coating a 10 mg/mL polymer solution onto a clean silicon wafer. Dynamic mechanical analysis (DMA) was performed using a TA Q850 instrument to obtain the storage modulus curves of the samples. The mesogen alignment of the films was observed using a polarized optical microscope (POM, Olympus BX53). One-dimensional (1D) small-angle X-ray scattering (SAXS) and two-dimensional (2D) wide-angle X-ray scattering (WAXS) patterns were recorded using a high-flux small-angle X-ray scattering instrument (SAXSess, Anton Paar) to characterize the microstructure and mesogen alignment. Uniaxial tensile tests were performed on a universal testing machine (SANS E42.503) at a tensile speed of 30 mm/min to obtain the stress-strain curves and mechanical parameters of the samples. The fatigue resistance of the materials was evaluated *via* 1000-cycle tensile tests using a TA Q850 DMA instrument at a constant strain of 200% at room temperature. The actuation stability was tested *via* isostrain cycling experiments on a TA Q850 DMA instrument with a fixed strain of 0.01% and a temperature range of 25–80 °C. The rheological properties of the materials were characterized using a Discovery HR20 rheometer (TA Instruments), which was operated in oscillation mode at an angular frequency of 10 rad/s and a strain of 1%, with the temperature ramped from 20 °C to 120 °C at a rate of 3 °C/min.

RESULTS AND DISCUSSION

Chemical Design of the Thermoplastic LCE

ABA-type PS-*b*-MCLCP-*b*-PS triblock copolymer was prepared *via* a two-step method. First, a dibromo-terminated MCLCP (Br-$MCLCP_{31}$-Br, M_n=23.8 kDa, PDI=1.36) macroinitiator was synthesized through thiol-ene click polymerization, end-capping modification and esterification (Fig. S1 in the electronic supplementary information, ESI). Styrene was then polymerized *via* ATRP using Br-MCLCP-Br as the macroinitiator,[27–29] yielding a series of PS-*b*-MCLCP-*b*-PS copolymers with different PS contents (Fig. 1a and Fig. S2 in ESI). The M_n and PDI values of the prepared copolymers were determined by GPC (Table S1 in ESI). According to the polymerization degree of the PS blocks, the three samples with different PS contents were named PS_{56}-*b*-$MCLCP_{31}$-*b*-PS_{56}, PS_{80}-*b*-$MCLCP_{31}$-*b*-PS_{80}, and PS_{141}-*b*-$MCLCP_{31}$-*b*-PS_{141}.

The incompatibility between the PS hard block and MCLCP soft block drives the microphase separation of the triblock copolymer (Fig. 1b). The MCLCP block forms a continuous elastic phase with controllable liquid crystal anisotropy, whereas the PS chains aggregate to form discrete hard domains that act as high-modulus physical crosslinking sites, replacing the permanent covalent crosslinks in conventional LCEs. This physical crosslinking structure not only provides a stable network for the elastomer to maintain structural integrity, but also endows the material with reprocessing and recyclability owing to the reversible dissociation and reconstruction of PS hard domains.

The thermal properties of PS-*b*-MCLCP-*b*-PS were systematically characterized *via* DSC, TGA, DMA, and rheological analyses. Taking PS_{80}-*b*-$MCLCP_{31}$-*b*-PS_{80} (PS content: 41 wt%) as an example, the DSC heating curve (Fig. 1c) shows two glass transition temperatures (T_g) at −6.4 and 94.3 °C, corresponding to the glass transitions of the MCLCP soft phase and the PS hard phase, respectively. A liquid crystal-isotropic phase transition (clear point, T_i) is observed at 68.2 °C on heating, which is the key temperature for thermally driven actuation. As shown in Fig. S8 (in ESI), the T_i of the samples shifted to higher temperatures with an increase in the PS content, because the denser physical crosslinking network formed by the higher PS content imposes stronger spatial confinement on the MCLCP segments, hindering the phase transition of the liquid crystal phase. Meanwhile, only one T_g corresponding to the MCLCP phase was observed at −9.4 °C on the DSC cooling curve, and the T_g signal of the PS phase was undetectable. This phenomenon is attributed to the disordered dispersion of the PS nanodomains in the MCLCP matrix, which results in a heterogeneous elastic network and broadens the relaxation time distribution of the PS segments.

The nanoscale morphology of PS-*b*-MCLCP-*b*-PS was investigated using AFM (Fig. 1d) and SAXS (Fig. S10 in ESI). The AFM results showed that the PS nanodomains were randomly dispersed in the continuous phase of the MCLCP. The SAXS profiles exhibit broad scattering peaks in the range of 0.2–0.4 nm^{-1} without any high-order diffraction peaks, indicating that

the system only exhibits microphase segregation without long-range ordered phase structures. The DMA results (Fig. 1e and Fig. S12 in ESI) and rheological analyses (Fig. S13 in ESI) show that all PS-*b*-MCLCP-*b*-PS samples exhibit a stable rubbery plateau above the clear point (T_i), which can effectively suppress the macroscopic flow of molecular chains and maintain the mechanical integrity of the materials during thermal actuation, which is a prerequisite for realizing reversible thermally driven deformation.

Reversible Thermally Driven Actuation Behaviors

The thermally driven actuation behavior of the PS-*b*-MCLCP-*b*-PS-based thermoplastic LCEs was systematically investigated. The polydomain PS-*b*-MCLCP-*b*-PS films were first prepared by solution casting using DCM as the solvent. After complete removal of the solvent, the films were uniaxially stretched to 200% strain and then subjected to isothermal annealing at 60 °C for 24 h in the stretched state. The annealing process induced the dissociation and reconstruction of the PS nanodomains, providing sufficient free volume for the mesogens to rearrange and align along the stretching direction, thus yielding monodomain PS-*b*-MCLCP-*b*-PS films with oriented mesogens (Fig. S14 in ESI).

The mesogen alignment of the annealed films was verified *via* 2D-WAXS (Fig. 2a and Fig. S16 in ESI) and POM (Fig. 2b and Fig. S15 in ESI). As shown in the POM images, all the stretched PS-*b*-MCLCP-*b*-PS films exhibited distinct bright-dark alternations when the sample stage was rotated by 45°. The corresponding 2D-WAXS results show anisotropic scattering rings, which are typical characteristics of uniaxially aligned mesogens. Notably, PS_{80}-*b*-$MCLCP_{31}$-*b*-PS_{80} showed sharp and regular diffraction rings corresponding to an order parameter (S) of 0.64, which was attributed to the balanced trade-off between the stability of the physical crosslinking network and the segment mobility of the MCLCP chains at this PS content, facilitating the highly uniform alignment of mesogens along the stretching direction.

The thermo-responsive deformation behavior of the monodomain films of PS-*b*-MCLCP-*b*-PS was investigated. Mesogen alignment and a stable crosslinked network are two key factors that endow LCEs with reversible thermally driven actuation behaviors.[30] The monodomain PS_{56}-*b*-$MCLCP_{31}$-*b*-PS_{56} films (S=0.58) failed to maintain structural stability during the test because the excessively low PS content led to insufficient anchoring of the physical crosslinking network, resulting in irreversible chain slip and creep upon heating. In contrast, PS_{80}-*b*-$MCLCP_{31}$-*b*-PS_{80} and PS_{141}-*b*-$MCLCP_{31}$-*b*-PS_{141} exhibited different thermodeformation behaviors (Figs. 2c and 2d). The monodomain PS_{80}-*b*-$MCLCP_{31}$-*b*-PS_{80} film (S=0.64) undergoes significant contraction with a maximum strain of 22.7% upon heating to 80 °C and fully recovers to its initial length when cooled back to room temperature (25 °C). This reversible thermally driven deformation could be repeated for multiple cycles with no obvious attenuation (Video S1 in ESI). However, the monodomain PS_{141}-*b*-$MCLCP_{31}$-*b*-PS_{141} film (S=0.43) shows irreversible thermo-induced contraction and cannot recover to its initial state after cooling. This is be-

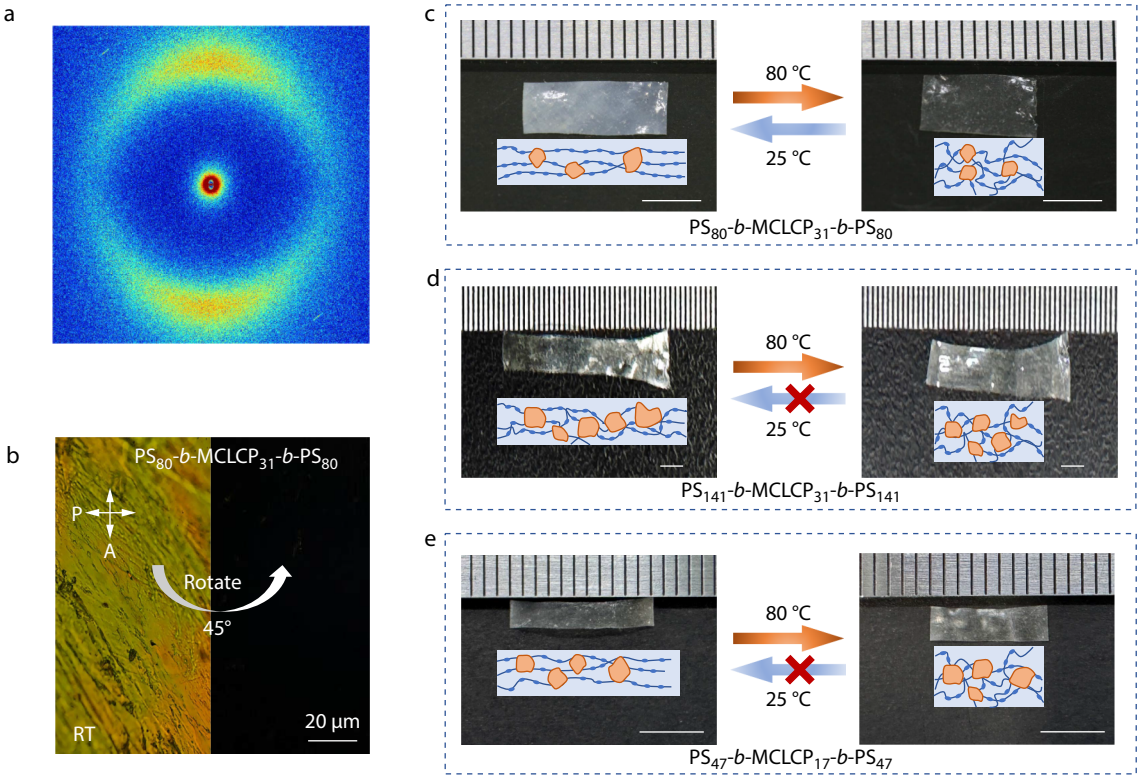

Fig. 2 (a) 2D-WAXS pattern at room temperature of the monodomain PS_{80}-*b*-$MCLCP_{31}$-*b*-PS_{80} film; (b) POM images of the monodomain PS_{80}-*b*-$MCLCP_{31}$-*b*-PS_{80} film; (c) Reversible actuation behaviors of the monodomain PS_{80}-*b*-$MCLCP_{31}$-*b*-PS_{80} film; (d) Irreversible actuation behaviors of the monodomain PS_{141}-*b*-$MCLCP_{31}$-*b*-PS_{141} film; (e) Irreversible actuation behaviors of the monodomain PS_{47}-*b*-$MCLCP_{17}$-*b*-PS_{47} film. All the scale bars are 5 mm.

https://doi.org/10.1007/s10118-026-3752-0

cause the excessively high PS content introduces strong spatial confinement on the MCLCP segments, making the material behave like plastics rather than elastomers, thus restricting the reversible rearrangement of mesogens.

In addition to the PS content, the molecular weight of the MCLCP block is a key factor that affects the reversible deformation of the materials. Control experiments showed that monodomain PS-*b*-MCLCP-*b*-PS samples with a low-molecular-weight MCLCP block (*e.g.*, PS-*b*-$MCLCP_{17}$-*b*-PS) did not exhibit reversible thermally driven deformation regardless of the PS content. As a typical example, although the monodomain PS_{47}-b-$MCLCP_{17}$-*b*-PS_{47} film possessed a highly aligned monodomain structure (S=0.68), it only exhibited irreversible contraction upon heating without spontaneous elongation during cooling (Fig. 2e). This is because the short MCLCP chains lack sufficient elasticity and segment mobility to realize the reversible rearrangement of mesogens under thermal stimulation. As a result, a long MCLCP chain with an appropriate content of PS hard blocks is necessary for PS-*b*-MCLCP-*b*-PS triblock copolymers to obtain reversible thermally driven actuation behaviors comparable to those of conventional chemically crosslinked LCEs.

Mechanical Properties

The mechanical properties of the polydomain PS-*b*-MCLCP-*b*-PS films were systematically investigated. As illustrated in Figs. 3(a) and 3(b), the elongation at break of the polydomain PS-*b*-MCLCP-*b*-PS films decreases gradually with an increase in the PS content, while the Young's modulus shows a monotonically increasing trend. Because the PS hard domains act as physical crosslinking points and reinforcing phases, a higher PS content leads to a higher crosslinking density and thus a higher modulus, but lower ductility. Specifically, PS_{56}-*b*-$MCLCP_{31}$-*b*-PS_{56} exhibited an ultrahigh elongation at break of over 800% with a Young's modulus of 8.36 MPa, reflecting the high ductility dominated by the soft MCLCP block. In contrast, PS_{141}-*b*-$MCLCP_{31}$-*b*-PS_{141} achieved a 2.3-fold increase in Young's modulus (19.59 MPa) owing to the significant reinforcement of the rigid PS domains, while its elongation at break decreased to about 300% because the excessively high crosslinking density severely restricted the mobility of the flexible MCLCP segments. Notably, the polydomain PS_{80}-*b*-$MCLCP_{31}$-*b*-PS_{80} film realizes an optimal balance between mechanical strength and flexibility, with a Young's modulus of 10.69 MPa, an elongation-at-break up to 680%, and the highest toughness of 90.33 MJ/m^3 among the three samples. This well-balanced mechanical performance provides the core structural basis for the excellent reversible thermally driven actuation performance.

The fatigue resistance and cyclic stability of the optimal polydomain PS_{80}-*b*-$MCLCP_{31}$-*b*-PS_{80} sample were further evaluated *via* 1000-cycle tensile tests with a constant 200% strain at room temperature (Fig. 3c). Obvious hysteresis loops, cyclic softening, and slight residual strain appear in the initial cycles, which is attributed to the mesogen rotation and energy dissipation through the partial tearing of PS domains under external stress. With an increase in the number of cycles, the area of the hysteresis loop gradually stabilized, and no obvious further cyclic softening or residual strain increase was observed, indicating that the PS physical crosslinking sites could establish a stable network under large strain. No irreversible structural damage occurred under long-term cyclic loading,

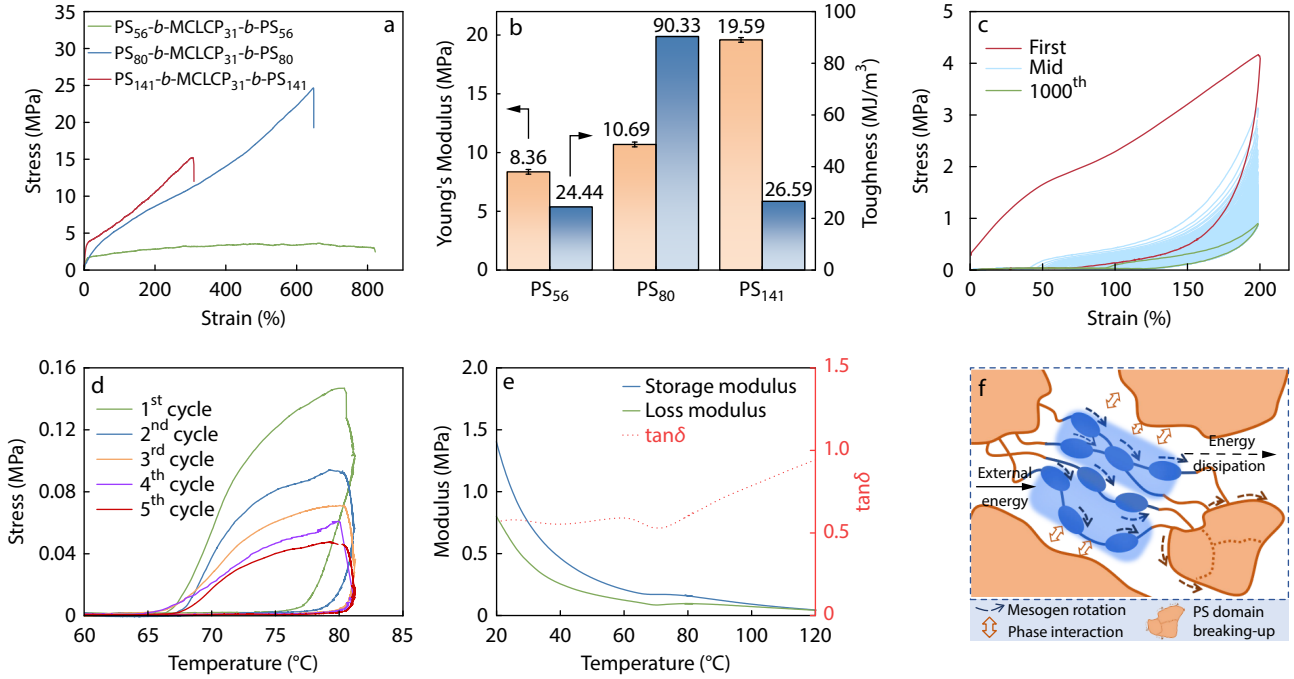

Fig. 3 (a) Stress-strain curves of the polydomain PS-*b*-MCLCP-*b*-PS films; (b) Young's modulus and toughness of the polydomain PS-*b*-MCLCP-*b*-PS films; (c) 1000-cycle tensile test of the polydomain PS_{80}-*b*-$MCLCP_{31}$-*b*-PS_{80} at 200% strain under room temperature; (d) Actuation stress of the monodomain PS_{80}-*b*-$MCLCP_{31}$-*b*-PS_{80} film under 0.01% isostrain testing; (e) Rheological test of shear storage modulus (G'), shear loss modulus (G'') and loss factor (tanδ) for the polydomain PS_{80}-*b*-$MCLCP_{31}$-*b*-PS_{80}; (f) Schematic illustration of the energy dissipation mechanism in PS-*b*-MCLCP-*b*-PS.

https://doi.org/10.1007/s10118-026-3752-0

demonstrating good fatigue resistance.

The cyclic thermally driven actuation of the monodomain PS_{80}-*b*-$MCLCP_{31}$-*b*-PS_{80} film with an order parameter of 0.64 was characterized *via* isostrain (0.01%) DMA tests in the temperature range of 25–80 °C. As shown in Fig. 3(d), the actuation stress of the sample increased rapidly above about 65 °C (consistent with the clear point from DSC results) and reached a maximum value at about 80 °C. The actuation stress decreases gradually from 0.14 MPa to 0.05 MPa after five actuation cycles, with the attenuation mainly concentrated in the first two cycles. The stress curve tended to stabilize in subsequent cycles. Temperature-dependent SAXS characterization was performed (Fig. S11 in ESI) to explain this phenomenon. The scattering profiles remained almost unchanged during the test, indicating that disordered PS domains were not reconstructed. Therefore, this stress attenuation is likely attributed to the structural relaxation of the polymer network under thermal stimulation. During the first two cycles, the polymer network underwent relaxation to release the internal residual stresses accumulated during the programming process. Driven by this stress release, a fraction of loosely anchored mesogens undergo spontaneous disorientation, leading to initial stress attenuation. Once this initial structural relaxation is completed, the physical crosslinking network reaches equilibrium, resulting in gradually stable actuation stress in subsequent cycles. Notably, the phase-transition temperature range remained unchanged throughout the five cycles, indicating that irreversible damage did not occur in the MCLCP chains. These findings also highlight the need for further molecular design strategies to enhance the mechanical properties and actuation stability of PS-*b*-MCLCP-*b*-PS-based LCEs in future work, such as introducing non-covalent interactions to strengthen the PS physical crosslinking domains.

The viscoelastic properties and damping performance of the polydomain PS_{80}-*b*-$MCLCP_{31}$-*b*-PS_{80} samples were characterized *via* parallel-plate rheology tests (Fig. 3e). Results show that no crossover between the shear storage modulus (G') and shear loss modulus (G'') was observed over the entire test temperature range of 20–120 °C, suggesting that the samples maintained the structural integrity of the physical crosslinking network and did not transition into a viscous liquid under the test conditions. In particular, the loss factor ($\tan\delta = G''/G'$) of the material remains above 0.3 in the whole test range, exhibiting good wide-temperature-range damping performance. Such damping performance originates from the synergistic energy dissipation of multiple mechanisms in the material (Fig. 3f), including the rotation of mesogens,[31] the physical tearing of large PS domains into smaller domains (a phenomenon that has been well documented in the structural evolution of thermoplastic elastomers),[32,33] and the interfacial friction between the PS hard domains and the MCLCP soft phase. These results further expand the application potential of the material in vibration damping, flexible buffer devices, and multifunctional smart responsive materials.

Reprocessing and Applications

A prominent advantage of physically crosslinked thermoplastic LCEs is their reprocessability and recyclability. The PS_{80}-*b*-$MCLCP_{31}$-*b*-PS_{80} LCE films can be efficiently recycled by solvent dissolution owing to the reversible dissociation of the PS block in organic solvents. As shown in Fig. 4(a) and Video S2 (in ESI), the PS_{80}-*b*-$MCLCP_{31}$-*b*-PS_{80} film was completely dissolved in organic solvents such as DCM to form a homogeneous solution. A

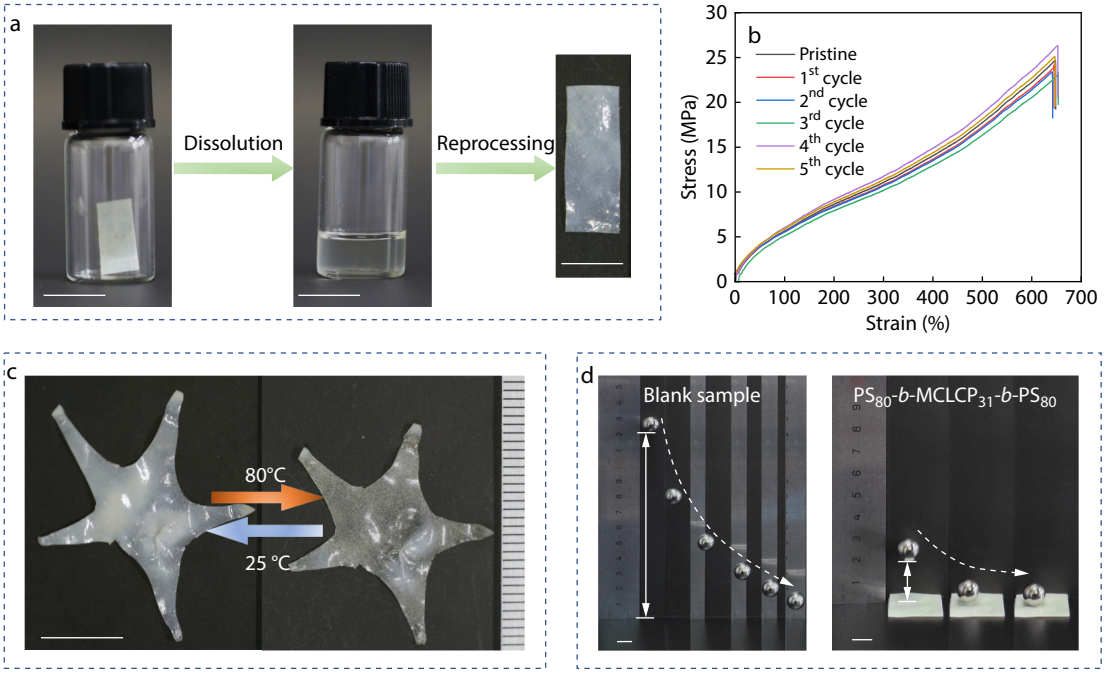

Fig. 4 Dissolution-reprocessing of PS_{80}-*b*-$MCLCP_{31}$-*b*-PS_{80} film; (b) Tensile test of recycled polydomain PS_{80}-*b*-$MCLCP_{31}$-*b*-PS_{80} films; (c) Reversible thermally driven actuation of the star-shaped actuator fabricated by PS_{80}-*b*-$MCLCP_{31}$-*b*-PS_{80}; (d) Verification of the damping effect of the polydomain PS_{80}-*b*-$MCLCP_{31}$-*b*-PS_{80} film *via* the falling ball test. All the scale bars are 10 mm.

new uniform film can be obtained by solution casting and solvent evaporation to realize the efficient recycling of the material. In contrast, conventional chemically crosslinked liquid crystal elastomer films only swelled in solvents and could not be dissolved in the solvent (Fig. S18 in ESI).

Uniaxial tensile tests were performed on the recycled films after multiple solvent dissolution-recasting cycles to evaluate the mechanical property retention after recycling. As shown in Fig. 4(b), the stress-strain curves of the recycled films after five recycling cycles were highly consistent with the pristine sample, with no significant attenuation of the elongation at break. Furthermore, the DSC analysis (Fig. S20 in ESI) revealed highly stable thermodynamic transitions across multiple cycles, confirming that the mesogens fully retained their inherent liquid crystalline characteristics. 1D-SAXS profiles (Fig. S21 in ESI) exhibited consistent broad scattering peaks at 0.2–0.4 nm^{-1}, verifying the reconstruction of the disordered microphase-separated structure. These results confirm that multiple solvent recycling cycles do not cause obvious degradation of the structure of the material and that the physical crosslinking structure can be reconstructed perfectly during the recasting process.

PS_{80}-*b*-$MCLCP_{31}$-*b*-PS_{80} LCE films can be freely shaped and reshaped into various functional actuators because of their thermoplasticity and reversible actuation performance. As a proof-of-concept, a star-shaped soft actuator was fabricated by stretching the five corners of the PS_{80}-*b*-$MCLCP_{31}$-*b*-PS_{80} film along their pointing directions and annealing at 60 °C for 24 h. As shown in Fig. 4(c), at room temperature (25 °C), the star-shaped actuator maintained its initial extended configuration. Upon heating to 80 °C, the liquid crystal-isotropic phase transition of the MCLCP block drives the actuator to undergo macroscopic shrinkage, presenting a contracted state (Video S3 in ESI). When the temperature decreased to 25 °C, the mesogens recovered to their initial oriented state, and the actuator fully recovered to its original extended shape, demonstrating the potential of the designed thermoplastic LCEs in the fabrication of soft actuators for soft robotics and smart devices.

In addition to the reversible thermally driven actuation performance, the polydomain PS_{80}-*b*-$MCLCP_{31}$-*b*-PS_{80} film exhibited excellent damping performance with a high tanδ over a broad temperature range, which was visually verified *via* a free-falling ball buffer test (Fig. 4d, Videos S4 and S5 in ESI). When a steel ball was dropped onto the PS_{80}-*b*-$MCLCP_{31}$-*b*-PS_{80} film, the ball only rebounded once at a height of approximately 2 cm and then stopped on the film. In contrast, the steel ball dropped onto the blank glass substrate showed an initial rebound height of 12 cm and stopped after multiple bounces. This result is in good agreement with previous rheological test results (tanδ > 0.3), directly demonstrating the remarkable damping effect of the material and its potential application in vibration damping and buffer devices.

CONCLUSIONS

In summary, we have proposed a chemical design strategy for physically crosslinked thermoplastic LCE based on ABA-type PS-*b*-MCLCP-*b*-PS triblock copolymers, in which dynamic physical crosslinking networks are formed by aggregated PS hard domains, replacing the permanent covalent crosslinks in conventional LCEs. We systematically investigated the regulatory effect of the PS block content on the network structure, mechanical properties, thermally driven actuation performance, and recyclability of the thermoplastic LCEs, and clarified the key structure-property relationships of the physically crosslinked LCEs. The thermoplastic LCE with a PS mass fraction of 41% (PS_{80}-*b*-$MCLCP_{31}$-*b*-PS_{80}) exhibited optimal comprehensive performance, realizing a delicate balance between the network confinement from the PS physical crosslinking domains and the segment mobility of the elastic LCP chains. This optimal sample integrated excellent reversible thermally driven actuation performance, well-balanced mechanical properties, and solvent recyclability. In addition, it exhibits a wide temperature-range damping performance owing to synergistic energy dissipation. A certain degree of stress and actuation performance attenuation during cyclic tests indicates the need for further molecular design optimization to enhance the long-term service stability of the materials, such as introducing non-covalent interactions to strengthen the physical crosslinking domains of PS. This work provides a feasible molecular design strategy for reprocessable and multifunctional LCEs and paves the way for their application in flexible actuators, artificial muscles, vibration-damping smart materials, and flexible wearable electronics.

Conflict of Interests

The authors declare no interest conflict.

Electronic Supplementary Information

Electronic supplementary information (ESI) is available free of charge in the online version of this article at http://doi.org/10.1007/s10118-026-3752-0.

Data Availability Statement

The data supporting the findings of this study are available from the corresponding author upon reasonable request.

ACKNOWLEDGMENTS

This work was financially supported by the National Natural Science Foundation of China (Nos. 52373173, 52473107 and 22307017), the Young Talent Support Program of Jiangsu Province (No. JSTJ-2024-433), and the Fundamental Research Funds for the Central Universities.

REFERENCES

1 White, T. J.; Broer, D. J. Programmable and adaptive mechanics with liquid crystal polymer networks and elastomers. *Nat. Mater.* **2015**, *14*, 1087–1098.
2 Jiang, Z. C.;Liu, Q.; Xiao, Y. Y.; Zhao, Y. Liquid crystal elastomers for actuation: a perspective on structure-property-function relation. *Prog. Polym. Sci.* **2024**, *153*, 101829.
3 Tang Y.; Pan, F.; Qin, L.; Yu, Y. Adaptive locomotion of pleurotya caterpillar-inspired segmental crawling robots with multiple

Graphical Abstract

Thermoplastic Liquid Crystal Elastomers Based on ABA-type Triblock Copolymers

Heng-Hui Zhu, Jin-Yu Wang, Nan-Kai Deng, Jia-Xiang Huang, Ya-Nan Hou, Meng Wang, Zhi-Yang Liu, and Shuai Huang

School of Chemistry and Chemical Engineering, Southeast University, Nanjing 211189, China

Thermoplastic liquid crystal elastomers are developed based on ABA-type PS-*b*-MCLCP-*b*-PS triblock copolymers, where polystyrene domains serve as physical crosslinking sites to enable reversible thermo-actuation and sustainable dissolution-reprocessing properties.

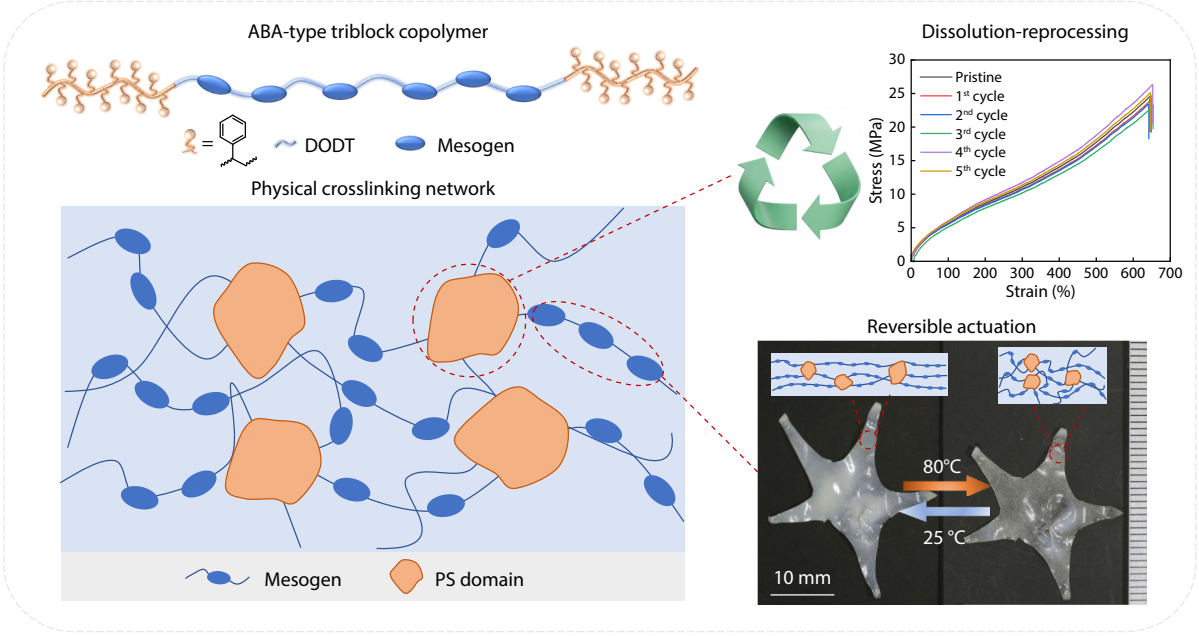

Chinese J. Polym. Sci., 2026 *https://doi.org/10.1007/s10118-026-3752-0*

postures. *Adv. Funct. Mater.* **2025**, *35*, 2506987.

4 Hu, J.; Nie, Z.; Wang, M.; Liu, Z.; Huang, S.; Yang, H. Springtail-inspired light-driven soft jumping robots based on liquid crystal elastomers with monolithic three-leaf panel fold structure. *Angew. Chem. Int. Ed.* **2023**, *62*, e202218227.

5 Wang, Z.; Si, M.; Han, J.; Shen, Y.; Yin, G.; Yin, K.; Xiao, P.; Chen, T. Hydrogen-bonded supramolecular network enabled gentle reprogramming of liquid crystal elastomer toward evolutionary robot. *Angew. Chem. Int. Ed.* **2025**, *64*, e202416095.

6 Zhang, C.; Muhetaer, R.; Zang, T. Z.; Fu, S.; Cheng, J. P.; Yang, L.; Wang, J.; Yang, K.; Fei, G. X.; Wang, Q. Y.; Lu, X. L.; Xia, H. S.; Zhao, Y. Investigating the influence of printing parameters on the helical deformation of 4D-printed liquid crystal elastomer fiber-actuators. *Chinese J. Polym. Sci.* **2025**, *43*, 605–615.

7 Wang, J. Y.; Bisoyi, H. K.; Huang, Y. L; Xu, Y. Y.; Zhang, X. F.; Huang S.; Li, Q. Collaborative actuation of liquid crystal elastomer unit cells as a function design platform. *Sci. China Mater.* **2025**, *68*, 236–243.

8 Liu, Q.; Chen, W. Single-fiber design for higher performance artificial muscles. *Adv. Mater.* **2026**, *38*, e14781.

9 Ding, J.; Liu, T.; Li, Y. Z.; Li, Q. N.; Zhu, L. Y. Locking alignment of liquid crystal actuators using hydrogen bonds to enable room-yemperature shape programmability and enhanced work capacity. *Adv. Funct. Mater.* **2025**, *35*, 2414510.

10 Liu, Z.; Hu X. N.; Bo R. H.; Shen, Z. M.; Zhang Y. H. A three-dimensionally architected electronic skin mimicking human mechanosensation. *Science* **2024**, *384*, 987–994.

11 Liu, C. Y.; Wang, Z. X.; Li, T. Y.; Yang, J. P.; Wang Z. J. Active pillar array structure by solvent-free liquid crystal elastomer resin. *Chinese J. Polym. Sci.* **2025**, *43*, 1012–1021.

12 Pei, Z.; Yang, Y.; Chen, Q.; Terentjev, E. M.; Wei, Y.; Ji, Y., Mouldable liquid crystalline elastomer actuators with exchangeable covalent bonds. *Nat. Mater.* **2014**, *13*, 36-41.

13 Saed, M. O.; Gablier, A.; Terentjev, E. M. Exchangeable liquid crystalline elastomers and their applications. *Chem. Rev.* **2022**, *122*, 4927–4945.

14 Zhu, Y. Y.; Xu, Z. T.; Wu, F. Y.; Wang, M.; Chen, L. Liquid-crystal elastomers based on covalent adaptable networks: from molecular design to applications. *Sci. China Mater.* **2023**, *66*, 3004–3021.

15 Liu, Y. W.; Liang, H.; Xu, H. T.; Xu, H. T.; Li, Z.; Ji, Y. Regulating actuations and shapes of liquid crystal elastomers through combining dynamic covalent bonds with cooling-rate-mediated control. *Chinese J. Polym. Sci.* **2024**, *42*, 1442–1448.

16 Zhang S. N.; Wang, Z. C.; Zhang, J. Y.; Liu, J. L.; Sun, C.; Qin, S. Y.; Ren, Y. X.; Zhang, L. Y.; Hu, W.; Yang, H. Healable and multi driving mode soft actuator enabled by disulfide-bonded liquid crystal elastomers. *Chem. Eng. J.* **2024**, *491*, 1385–8947.
17 Huang, S.; Shen, Y. K.; Bisoyi, H. K.; Yu, T.; Liu, Z. C.; Wang, M.; Yang, H.; Li, Q. Covalent adaptable liquid crystal networks enabled by reversible ring-opening cascades of cyclic disulfides. *J. Am. Chem. Soc.* **2021**, *143*, 12543–12551.
18 Liu, Y.; Yang, Q.; Liu, Q.; Hou, J. B.; Zhao, J.; Zhang, Y.; Peng, Q. Y.; Jiang, Z. C.; Xiao,Y. Y.; Zeng, H. B. Tailoring Diels–Alder cross-linked liquid crystal elastomers for spatially programmable monolithic actuators. *ACS Macro Lett.* **2025**, *14*, 495–501.
19 Xu, Z. T.; Zhu, Y. Y.; Ai, Y.; Yuan Z. Y.; Li, C. Q.; Zhou, D.; Chen, L. Synchronous differential orientation of liquid crystal elastomers based on dual dynamic covalent bonds. *J. Mater. Chem. A* **2025**, *13*, 13091–13099.
20 Zhao, X.; Chen, Y.; Peng, B.; Wei, J.; Yu, Y. L. A Facile strategy for the development of recyclable multifunctional liquid crystal polymers *via* post-polymerization modification and ring-opening metathesis polymerization. *Angew. Chem. Int. Ed.* **2023**, *135*, e202300699.
21 Xu, Z. W.; Xing C.; Li, W. H. Microscopic origins of the distinct mechanical response of ABA and ABC block copolymer nanostructures. *ACS Macro Lett.* **2024**, *13*, 240–246.
22 Ruzette, A. V.; Leibler, L. Block copolymers in tomorrow's plastics. *Nat. Mater.* **2005**, *4*, 19–31.
23 Hayashi, M.; Matsushima, S; Noro, A.; Matsushita, Y. Mechanical property enhancement of ABA block copolymer-based elastomers by incorporating transient cross-links into soft middle block. *Macromolecules* **2015**, *48*, 421–431
24 Wang, W. Y.; Lu, W.; Goodwin, A.; Wang, H. Q.; Yin, P. C.; Kang, N. G.; Hong, K. L; Mays, J. W. Recent advances in thermoplastic elastomers from living polymerizations: macromolecular architectures and supramolecular chemistry. *Prog. Polym. Sci.* **2019**, *95*, 1–31.
25 Lang, C.; Lloyd, E. C.; Matuszewski, K. E.; Xu, Y. F.; Ganesan, V.; Huang, R.; Kumar M.; Hickey, R. J. Nanostructured block copolymer muscles. *Nat. Nanotechnol.* **2022**, *17*, 752–758.
26 Yang, J. X.; Zhang, X. L.; Yin, L.; Jiang, J.; Zhao, Y.; Li, Y.; Han, L. Dual physically crosslinked azobenzene liquid crystal elastomers programmable for multi-modal information encryption. *Chem. Eng. J.* **2025**, *507*, 1385–8947.
27 Cai F.; Yang, B. W.; Lv, X. D.; Feng, W.; Yu, H. F. Mechanically mutable polymer enabled by light. *Sci. Adv.* **2022**, *8*, eabo1626.
28 Matyjaszewski, K.; Tsarevsky, N. Nanostructured functional materials prepared by atom transfer radical polymerization. *Nat. Chem.* **2009**, *1*, 276–288.
29 Dau, H.; Jones, G. R.; Tsogtgerel, E.; Nguyen, D.; Keyes, A.; Liu, Y. S.; Rauf, H.; Ordonez, E.; Puchelle, V.; Alhan, H. B.; Zhao, C.; Harth, E. Linear block copolymer synthesis. *Chem. Rev.* **2022**, *122*, 14471–14553.
30 Fang, H. G.; Zhang, F.; Zhao Y. P.; Gao, X. C.; Zhou, W. J.; Qi, G. B.; Ding, Y. S.; Winter, H. H. Rheology of smectic liquid crystalline elastomers with dynamic covalent bonds. *Macromolecules* **2023**, *56*, 7808–7817.
31 Choi, S.; Guo, H. Y.; Kim, B.; Seo, J. H.; Terentjev, E. M.; Saed, M. O.; Ahn, S.; K. Harnessing extreme internal damping in polyrotaxane-incorporated liquid crystal elastomers for pressure-sensitive adhesives. *Adv. Funct. Mater.* **2025**, *35*, 2413824.
32 Qi, H. J.; Boyce, M. C. Stress-strain behavior of thermoplastic polyurethanes. *Mech. Mater.* **2005**, *37*, 817–839.
33 Wang, M.; Yu J. H.; Tian, Y. S.; Wang, J. D.; Qin, X.; Lu, Y. L. Mechanical-fatigue-driven hierarchical structural evolution in polyurethane elastomers with different hard segment contents. *Macromolecules* **2026**, *59*, 2206–2217.

https://doi.org/10.1007/s10118-026-3752-0